ARTICLE

Reactivity of the Antitumor Complex (H$_2$trz)[*trans*-RuCl$_4$(N^2-Htrz)$_2$] in the Presence of DNA Purines within a Fluorinated Silica Matrix

Luís M. F. Lopes,[†] Maximilian N. Kopylovich,[‡] Armando L. Pombeiro,[‡] and Laura M. Ilharco[*,†]

[†]CQFM, Centro de Química-Física Molecular, and IN, Institute of Nanoscience and Nanotechnology, Instituto Superior Técnico, Universidade Técnica de Lisboa, Av. Rovisco Pais 1, 1049-001 Lisboa, Portugal

[‡]CQE, Centro de Química Estrutural, Instituto Superior Técnico, Universidade Técnica de Lisboa, Av. Rovisco Pais 1, 1049-001 Lisboa, Portugal

S *Supporting Information*

ABSTRACT: The stability of the antitumor Ru(III) complex (H$_2$trz)-[*trans*-RuCl$_4$(N^2-Htrz)$_2$] within a tailored sol—gel silica matrix was studied, combining the information from UV—vis and infrared spectroscopies. The matrix was synthesized by a one-step sol—gel process catalyzed by hydrofluoric acid, resulting extremely light, hydrophobic and fluorinated. It is shown that upon encapsulation, the complex undergoes a series of processes, starting with the increase in charge density on the metal center, followed by hydrolysis reactions. The modified complex interacts with the matrix through hydrogen bonds between the aquo/hydroxo ligands and the fluorine atoms. Its interactions with DNA purines (guanine and adenine) were probed within the confined medium defined by the same silica matrix. It is found that coencapsulated guanine does not interfere with the complex aquation processes, while coencapsulated adenine has a delaying effect. No covalent bonding between the complex and the purines is detected, but interactions between the triazole ligands and the imidazole ring of guanine and the imidazole and pyrimidine rings of adenine are observed. Hydrogen bonding is established between the carbonyl and the ammine groups of guanine and the aquo/hydroxo ligands of the complex. For adenine, those interactions involve mostly the N9H of the purine and the NH groups of the triazole ligands, in addition to $\pi-\pi$ interactions.
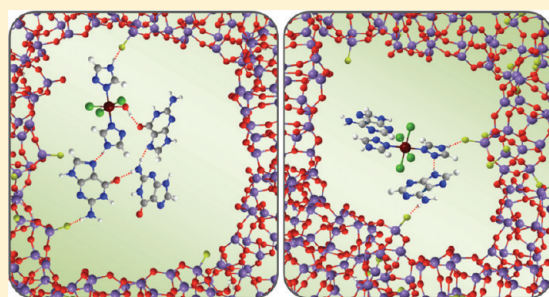
1. INTRODUCTION

The success obtained in the treatment of cancer using platinum-based compounds has stimulated the research on other transition metal compounds, looking for lower toxicity and higher specificity.[1] Whereas nickel and palladium complexes are too kinetically reactive to be used as drugs, those of iridium and osmium are in general too inert. Ruthenium and rhodium have produced the most promising compounds.[2−4] Among these, Ru(II) and Ru(III) complexes have emerged as the more important nonplatinum alternatives: the azole-based Ru(III) complexes, such as NAMI-A (imidazolium *trans*-imidazole dimethyl sulfoxide tetrachlororuthenate) and KP1019 (indazolium *trans*-[tetrachlorobis (1*H*-indazole)ruthenate(III)]) are the most successful examples, having been the first to reach clinical trials.[5−12]

The forms of ruthenium complexes detected in the coordinated biomolecules were different from those originally introduced in the organism, which suggests that these complexes may act as pro-drugs. The mechanisms behind these transformations may involve ligand substitution and redox processes occurring in the blood or inside the cells.[13] Some extrapolations concerning the behavior of antitumor Ru(III) complexes were based on similarities with Fe(III), namely in the high affinity for transferrin, which could be responsible for the accumulation of Ru(III) complexes in the tumors.[14] A widely accepted hypothesis for the activity of Ru

complexes is the reduction of the Ru(III) center to Ru(II), favored by the reductive environment inside the tumor. Naturally, to be eligible as pro-drugs, these compounds must possess biologically accessible reduction potentials. This reduction process increases the lability of the ligands, mainly of chloride, and consequently the reactivity of the complexes.[3] Under such conditions, aquation becomes another important reaction responsible for their activation.[14,15] The hydrolysis may be promoted by an increase of electron donation from the neutral ligand to the metal, with simultaneous weakening of the metal—chloride bonds. Therefore, an increase in the basicity of the azole ligands promotes the complex lability toward dechlorination. The replacement of a Cl$^-$ ligand results in a positive shift of the reduction potential, thus favoring the Ru(III) → Ru(II) conversion.[16] In general, the aquo complexes formed are significantly more reactive, and are therefore considered to be the actual species responsible for the antitumor activity. This is corroborated by the experimental evidence that only "aged" solutions react with DNA and with other biological targets.[17] Further hydrolysis products may include di- or polynuclear (μ-oxo) Ru complexes, whose formation is pH dependent,
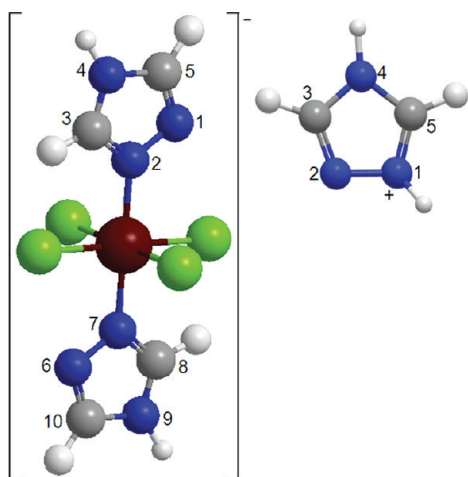
Figure 1. Ball and stick model of the $[trans\text{-}RuCl_4(N^2\text{-}Htrz)_2]^-$ complex and its counterion (1,2,4-triazolium), optimized by the Gaussian module of Chem 3D Ultra 10.0.

with hydrolysis proceeding faster at higher pH.[18] The study of the hydrolysis processes of Ru complexes in different media is still a priority, in order to identify the products and better understand their mode of action in the organism.

A common drawback of these complexes is their poor water solubility, which is an essential requirement for pharmaceutical formulation. In an attempt to overcome this limitation, several ligands have been tested. 1,2,4-Triazole ligands are particularly interesting, because they are structurally similar to those of the successful antitumor Ru complexes NAMI-A and KP1019, may adopt different coordination modes,[10] and have the ability to bridge metal ions together in different geometries.[19]

The present work focused on the triazolium-[*trans*-tetra-chlorobis(1*H*-triazole)ruthenate(III)]: (H₂trz)[*trans*-RuCl₄-(N²-Htrz)₂], here referred as *trans*-Htrz. Although the *cis* isomer form possesses better water solubility, it has been proven that the *trans* form (Figure 1) has a higher antiproliferative activity in vitro toward three human colon and mammary carcinoma cell lines.[20]

The best way to study the interactions of this complex with DNA bases, namely the purines, is to favor the encounter between the two molecules within a confined environment. For ruthenium nitrosylnitrate and ruthenium ammine complexes, nanostructured, hydrophilic, and relatively dense silica matrices, synthesized by a two-step sol gel process, using HCl as hydrolysis catalyst, proved to be suitable for this purpose.[21,22]

In the present work, with the aim of minimizing the interactions of the encapsulated molecules with the matrix and thus enhance the interactions between them, a different matrix was synthesized by a one step sol−gel process catalyzed by hydrofluoric acid. The study of the interactions between the complex and each DNA purine was preceded by an evaluation of the complex stability within the resulting matrix, which is fluorinated, hydrophobic and extremely light.

2. EXPERIMENTAL SECTION

2.1. Materials. The ruthenium complex, (H₂trz)[*trans*-RuCl₄-(N²-Htrz)₂], was synthesized adapting the experimental procedure describe elsewhere.[20]

Table 1. Relevant Molar Ratios and Identification of the Samples

sample[a]	molar ratios		
	purine/TEOS	complex/TEOS	purine/complex
control SiO₂	-	-	-
Ade/SiO₂	0.011	-	-
Gua/SiO₂	0.011	-	-
trans-Htrz/SiO₂	-	0.0037	-
Ade/*trans*-Htrz/SiO₂	0.011	0.0037	3.0
Gua/ *trans*-Htrz/SiO₂	0.011	0.0038	2.9

[a] Gua, guanine; Ade, adenine.

Tetraethoxysilane (TEOS, 98%), adenine (99%) and guanine (99.9%, pure) were purchased from Sigma-Aldrich. Hydrofluoric acid (HF, 40%, diluted to 3%) used as catalyst, and 2-pronanol (99.8%) were obtained from Fluka. All chemicals were used without further purification. Distilled water was used in all the sol−gel synthesis.

2.2. Preparation of the Sol−Gel Matrix. All the matrices were synthesized by a one-step sol−gel process. The appropriate amount of ruthenium complex was weighed to a polypropylene container and dissolved with an HF 3% aqueous solution (6.50 mL; 1.1 mmol), under stirring, until a homogeneous solution was obtained. The cosolvent, 2-propanol was then added (6.30 mL; 82.4 mmol), and the mixture vigorously stirred. Finally, the silica precursor, TEOS (2.00 mL; 8.97 mmol), was added dropwise, under stirring. The complex concentration in the final solution was 2.2 mM, and the pH ∼1. The container with the reaction mixture was sealed and placed at 20 °C, sheltered from light, under stirring (140 rpm) for 40 min (time required for gelling).

After an aging period of 48 h at 20 °C, the container was opened and the gel left to dry for 1 week at 20 °C and ambient pressure, and 2 weeks at 20 °C under progressive vacuum down to 10−4 mbar, sheltered from light.

For encapsulation of the purines (and coencapsulation with the Ru complex), a similar procedure was followed, replacing the HF 3% solution for a 0.016 M stock solution of each base, prepared as follows: the weighed amount of purine was dissolved in a 3% HF solution (at room temperature for adenine and at ∼90 °C for guanine), under vigorous stirring, until a colorless and clear solution was obtained (∼1 h). All the final solutions were yellowish, except that containing adenine and *trans*-Htrz, which was orange.

In all the samples the H₂O/TEOS, 2-PrOH/TEOS, and HF/TEOS molar ratios were kept as 40, 9.2, and 0.12, respectively. Other important molar ratios are indicated in Table 1.

2.3. Characterization. Infrared analysis of all the samples was performed by diffuse reflectance infrared Fourier transform (DRIFT) spectroscopy, using a Mattson RS1 FTIR spectrometer with a Specac Selector, in the 400−4000 cm⁻¹ range (wide band MCT detector), at 4 cm⁻¹ resolution. The spectra were the result of 500 coadded scans for each sample, ratioed against the same number of scans for the background (ground KBr, FTIR grade, from Aldrich). All the solids were previously ground and mixed with KBr in appropriate proportions to obtain spectral absorbance in the range of applicability of the Kubelka−Munk transformation.[23] Since the dopants' contents were very low, two sample/KBr ratios were used, the lower one for the spectral analysis
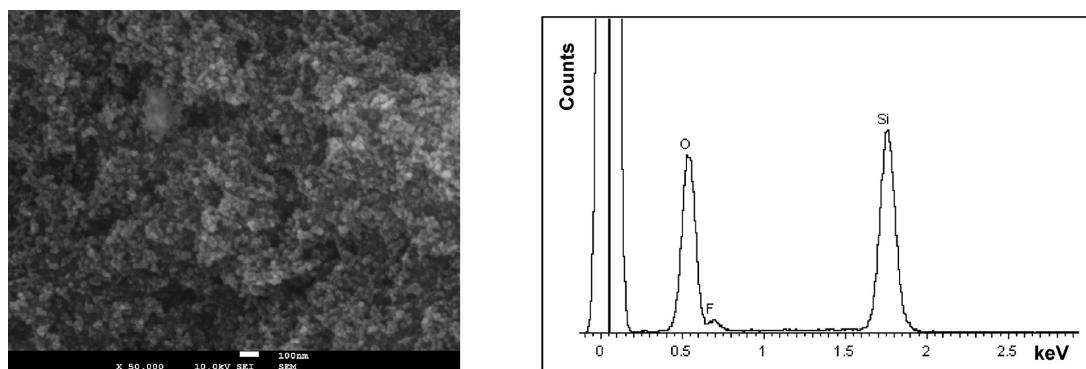
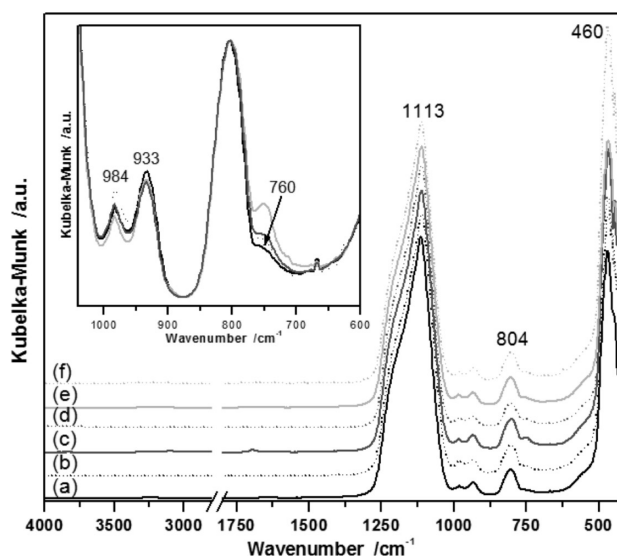**Figure 2.** SEM microphotograph and EDS−SEM spectrum of the control silica matrix.

Figure 3. DRIFT spectra of the fluorinated silica matrices with and without encapsulated dopants, vertically translated for better comparison: (a) control SiO_2; (b) *trans*-Htrz/SiO_2; (c) Ade/SiO_2; (d) Ade/*trans*-Htrz/SiO_2; (e) Gua/SiO_2; (f) Gua/*trans*-Htrz/SiO_2. The spectra were normalized to the maximum absorption, at ~1113 cm^{-1} (ν_{as}Si−O−Si mode). Inset: detail of some spectra in the 1050−600 cm^{-1} region, normalized to the ν_sSi−O−Si mode.

of the silica matrix and the higher one to characterize the encapsulated molecules.

UV−vis spectra of the powdered samples were recorded in diffuse reflectance mode (DRUV), using a Shimadzu UV-3101PC double-beam spectrophotometer, with a coupled MPC-3100 unit, equipped with an integrating sphere coated with $BaSO_4$. The range from 280 to 800 nm was covered. The baseline was recorded using a $BaSO_4$ reference (Wako Pure Chemical Industries). The absorption spectra of the ground state species were obtained using the Kubelka−Munk function. For comparison, the UV−vis spectrum of the Ru complex in acid solution ([HCl] = 0.08 M) was also recorded.

The microstructure of the control matrix was observed by scanning electron microscopy (SEM). Fractured surfaces were examined with a FEG-SEM microscope JEOL JSM-7001F operated at 10 keV. The surfaces were previously sputter coated with a gold layer ~200 Å thick, to avoid charging effects during observation. A complementary semiquantitative elemental analysis was

performed before coating, using an energy dispersive X-ray spectroscopic (EDS) detector for light elements from ThermoNoran.

Envelope density measurements of the dried samples were carried out in a Geopyc 1630 (Micromeritics) using Dryflo as free-flowing dry medium and a consolidation force of 15 N for 15 measurement cycles. All the samples were evacuated to 9×10^{-7} mbar at room temperature before being weighed.

N_2 adsorption−desorption isotherms (at 77 K) were obtained using an ASAP 2020 (Micromeritics) apparatus.

3. RESULTS AND DISCUSSION

3.1. The Silica Matrix. In order to minimize the decomposition of the complex during encapsulation, a one-step sol−gel synthesis was followed, using hydrofluoric acid as catalyst, since it acts as a nucleophile that simultaneously induces hydrolysis of the silica precursor and promotes condensation of the hydrolyzed species.[24] It allows reducing the time required for gelation and the exposition of the Ru-complex to the sol−gel mixture.[18]

The three-dimensional microstructure of the matrix, with a network of macropores (Figure 2), is responsible for its extremely low envelope density (0.414 ± 0.002 g·cm^{-3}, which allows considering this matrix as an aerogel), and is consistent with the low specific surface area deduced from the BET analysis of the N_2 sorption isotherms (96 m^2·g^{-1}). Matrix fluorination is unequivocally established by the semiquantitative elemental analysis EDS−SEM (Figure 2).

The molecular structure of the control silica matrix and any perturbations induced by encapsulation of the Ru-complex, the purine bases and both were assessed by analysis of their DRIFT spectra, shown in Figure 3.

The control silica is characterized by extensive condensation, as shown by the high yield in siloxane bridges: very strong ν_{as}(Si−O−Si) band at 1113 cm^{-1}, accompanied by the ν_s(Si−O−Si) mode, at 804 cm^{-1}. The extremely weak region between 3700 and 2800 cm^{-1} (where ν(O−H) bands would be expected) shows irrelevant contribution from either residual silanol groups or adsorbed water, which would also be responsible for a band at ~1650 cm^{-1} (δ(HOH)). Fluorination is confirmed by the appearance of ν(Si−F) bands in the DRIFT spectrum: although some contribution from ν(Si−OH) and ν(Si−O−) modes (expected between 930 and 960 cm^{-1}) could exist, taking into account the low content in silanol groups, the band at 984 cm^{-1} is mostly assigned to the ν_s(Si−F) modes of $O_{2/2}SiF_2$ and $O_{1/2}SiF_3$ tetrahedral species, and the one at
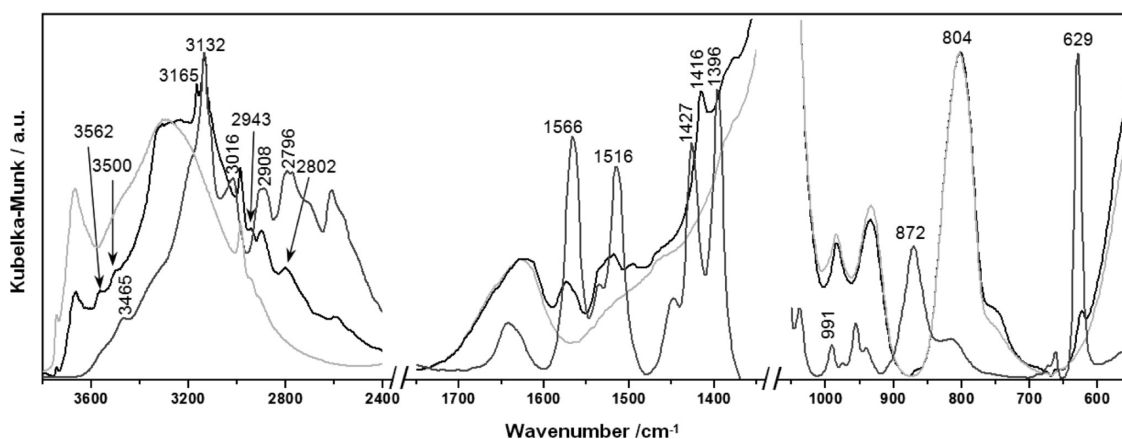
Figure 4. Three regions of the DRIFT spectra of polycrystalline *trans*-Htrz (gray), encapsulated *trans*-Htrz (black) and control SiO$_2$ (light gray). In each region, the spectra of *trans*-Htrz and *trans*-Htrz/SiO$_2$ samples were normalized to the maximum absorption, in order to balance the low complex content, and the spectrum of control SiO$_2$ was normalized to the maximum absorption of silica.

Table 2. Total Pore Volume (V_p) and Specific Surface Area (S_{BET}) of the Silica Matrices

sample	$V_p/cm^3 \cdot g^{-1}$	$S_{BET}/m^2 \cdot g^{-1}$
control SiO$_2$	0.491	96
Ade/SiO$_2$	0.584	124
Gua/SiO$_2$	0.517	132
trans-Htrz/SiO$_2$	0.583	103
Ade/*trans*-Htrz/SiO$_2$	0.408	88
Gua/*trans*-Htrz/SiO$_2$	0.866	125

933 cm^{-1} to O$_{3/2}$SiF species (inset in Figure 3 and Table 3).[25] Moreover, the shoulder at 760 cm^{-1} is characteristic of fluorinated silica and corresponds to the νSi—F mode in O$_{4/2}$SiF species with intermediate geometry between tetrahedral and octahedral, or to the ν(Si—O—Si) mode of relaxed bonds due to the occurrence of strongly polarized Si—F bonds in its vicinity.[26,27]

The strong band at 460 cm^{-1} is characteristic of a rocking mode of the oxygen atoms perpendicular to the Si—O—Si plane, plus some Si cation motion.[28] The ν_{as}(Si—O—Si) band is very narrow (half-width of 170 cm^{-1}), indicative of a homogeneous distribution of elementary siloxane rings. The band deconvolution in a sum of Gaussian components in the 1000—1300 cm^{-1} region (available as Supporting Information, Figure S1 and Table S1) yielded a largely predominant population of four member units, (SiO)$_4$, ($\sim$74%), with a small splitting between the longitudinal—optic and transverse—optic components (LO—TO splitting of $\sim$36 cm^{-1}). This is associated with a highly porous structure,[29] and is consistent with the extremely low envelope density determined, with predominance of macropores

The DRIFT spectra show that incorporation of the Ru complex and/or purine bases does not influence the structure of the matrix, at a molecular level: it remains hydrophobic and the profile of the silica fingerprint band (ν_{as}Si—O—Si) does not change, suggesting that the dominant elementary siloxane rings are of the same type. However, the shoulder at 760 cm^{-1} becomes better resolved and shifts to lower wavenumbers, beyond the spectral resolution.

Although the encapsulated molecules induce only a slight increase in the envelope density of the matrix (ρ_e ranges between 0.45 and 0.55 g cm^{-3}), their influence on the pore structure is

clear (Table 2): the specific surface areas (S_{BET}) obtained from BET analysis of the N$_2$ sorption isotherms are higher than that of the control silica, confirming a decrease in the average dimensions of the macropores by influence of the individual dopants. In the case of *trans*-Htrz, the higher total pore volume (V_p) without the corresponding increase in surface area suggests a different pore morphology. Co-encapsulated molecules have very different effects on the matrix: while the pair Ade/complex only seems to induce a silica structure with more filled macropores, the pair Gua/complex strongly affects the pore shape. These matrix modifications are correlated with different types of interactions between the complex and the two purines.

3.2. Comparison between the Stability of (H$_2$trz)[*trans*-RuCl$_4$(N^2-Htrz)$_2$] within the Silica Matrix and in Aqueous Solution. The modifications on the complex structure in solution and induced by encapsulation were evaluated both by UV—vis and infrared spectroscopies.

The infrared spectrum of polycrystalline (H$_2$trz)[*trans*-RuCl$_4$-(N^2-Htrz)$_2$] deserves a brief analysis, since it has not been published so far. The full DRIFT spectrum is shown in Supporting Information (Figure S2), and significant regions are included in Figure 4.

The proposed band assignments are summarized in Table 3. They take into account the vibrational spectrum of 1,2,4-triazole in different physical states (obtained in this work and published), and theoretical calculations using various potential energy distributions.[30−32] In this particular complex the ligand is stabilized in the 4H tautomeric form and binds to Ru(III) via N2,[20] whereas the most stable forms of free 1,2,4-triazole are 1H and 2H.[33]

The bands at 629 and 3134 cm^{-1} are the fingerprints of the (H$_2$trz)[*trans*-RuCl$_4$(N^2-Htrz)$_2$] complex, and are assigned to ring torsion and CH stretching modes, respectively.[20] The weak band at 3465 cm^{-1}, assigned to the stretching mode of weakly hydrogen bonded NH groups, is a proof that there are very few such groups in the crystalline state. Because of the contribution of the two triazole ligands, as well as the triazolium counterion, a broad νNH band appears, with different components (with maxima at 2908, 2887, 2796, 2773, and 2611 cm^{-1}) as a result of intermolecular NH···N hydrogen bonds. For the same reason, the NH out-of-plane bending, expected at 540 cm^{-1} in the isolated 1,2,4-triazole molecule,[31] shifts to higher frequencies (maxima at 976, 956, and 941 cm^{-1}). The in-plane NH bending

Table 3. Proposed Band Assignments of the DRIFT Spectra of Polycrystalline and Encapsulated (H$_2$trz)[$trans$-RuCl$_4$(N^2-Htrz)$_2$] and Comparison with 1,2,4-Triazole Powder^a

			1,2,4-triazole	
$trans$-Htrz	$trans$-Htrz/SiO$_2$	proposed band assignments	this work	ref 31,32
	3740$_{vw}$/3662$_{vw}$	ν(O−H) (~free), silica		
	3562$_{vw}$	ν(O−H) (~free), aquo/hydroxo ligands		
3465$_w$	3500$_{vw}$	ν(N−H) (free or weakly H bonded)		
~3329/~3186$_{sh}$		ν(N−H) (weakly H bonded)		
	~3300$_{vw,br}$	ν(O−H) (H bonded)		
3134$_S$	3165$_{vw}$/3132$_{vw}$	ν(=C−H)	3128$_S$	3124$_S$
~3111$_{sh}$/3016$_m$			3120$_w$/3095/3033	3116$_S$
2908$_m$	2943$_{vw}$	ν(N−H) (H bonded)	2927/2910$_S$	
2887$_m$	2899$_{vw}$		2866/2837$_S$	
2796$_m$	2802$_{vw}$		2822/2791$_S$	
2773$_m$			2773/2750$_S$	2730$_{VS}$
~2702$_{sh}$			2735/2698	
2611$_m$			2656$_w$	
2362$_w$/2343$_w$		combination bands		
1566$_m$	1574$_{vw}$/1562$_{sh}$		1766$_w$	1830$_m$
1535$_w$	~1533$_{vw,sh}$		1543/1531$_m$	1547/1535$_m$
1516$_m$	1518$_{vw}$	δ(CH+ring stretch) (N2−C3, N4−C5, C3−N4)		
	1496$_{vw}$	ring stretch	1483$_{VS}$	1488$_{VS}$
1448$_w$		combination band		
1427$_m$	1416$_w$	ring stretch (N2−C3, N4−C5, N1−N2, N1−C5)		
1396$_m$	1377$_{vw,sh}$	ring stretch (N1−N2, N1−C5) + δ(NH)	1379$_m$	1383$_m$
		combination band	1362/1333$_w$	1364$_w$
1302$_m$			1302$_w$	1304$_m$
1263$_w$		δ(CH) in-plane	1271$_{VS}$	1272$_{VS}$
		ring stretch (C3−N4) + δ(CH)	1257$_S$	1260$_{VS}$
1194$_w$		δ(NH) in-plane	1180$_m$	1184$_m$
1153$_m$		ring breathing	1147$_{VS}$	1146$_S$
1122$_m$		δ(NH) in-plane		
	1113$_{VS}$	ν_{as}(Si−O−Si)		
1055$_S$		δ(CH)	1059$_S$	1058$_m$
1039$_S$/991$_m$		ring bend		
	984$_w$	ν(Si−F$_2$) (O$_{2/2}$SiF$_2$) and ν(Si−F$_3$) (O$_{1/2}$SiF$_3$) tetrahedral species		
976$_w$		ring bend	982$_{VS}$	982$_{VS}$
956$_m$		ring bend/γ(NH) out-of-plane	957$_S$	968/957$_m$
941$_m$		γ(NH) out-of-plane + γ(CH)	926$_S$	943/934$_m$
	933$_w$	ν(Si−F) (O$_{3/2}$SiF)		
872$_S$/816$_m$	~868$_{sh}$	γ(C−H) out-of-plane	885$_{VS}$	892/885$_m$
	804$_m$	ν_sSi−O−Si		
	760$_{sh}$	νSi−F (O$_{4/2}$SiF)		
661$_w$	~660$_{sh}$	τ(ring) + γ(CH)	680$_{VS}$	684$_m$
		τ(ring)	649$_S$	652$_m$
629$_{VS}$	623$_w$	τ(ring) + γ(NH)		
530$_m$		ν(Ru−N)		
	460$_{VS}$	ρ(O, $\perp$ Si−O−Si plane)		

^{a} Key: VS, very strong; S, strong; m, medium; w, weak; vw, very weak; br, broad.

is not a localized mode, even in the free 1,2,4-triazole molecule. It contributes essentially to the band at 1122 cm^{-1}. Different ring stretching modes are observed, at 1427, 1396, and 1153 cm^{-1} (breathing), as well as ring bending modes, at 1039 and 991 cm^{-1}. The Ru−N characteristic stretching is observed at 530 cm^{-1}.

Within the matrix, the strong νC−H band (3134 cm^{-1}) splits in two components (at 3165/3132 cm^{-1}), suggesting the

existence of different neighborhoods to the triazole ligands. Also the changes in the band profile and the shifts observed in the triazole ring stretching modes ($1750-1350$ cm^{-1} region) are attributed to ring deformations due to confinement within the matrix or to perturbations induced by partial ligand replacement. This is particularly clear for the bands at 1427 and 1396 cm^{-1} that shift to 1416 and 1377 cm^{-1}, respectively, upon encapsulation. The strong ring torsion appears shifted to 623 cm^{-1}, which is also compatible with the proposed perturbations.

The NH groups become more weakly hydrogen bonded, since all the νN−H bands shift to higher wavenumbers: from 3456, 2908, 2887, and 2796 cm^{-1} to 3500, 2943, 2899, and 2802 cm^{-1}, respectively. This suggests that NH···N interactions between complex molecules in the crystalline phase are broken and not replaced by equally strong ones. Therefore, the complex is entrapped either as a single molecule or as loosely hydrogen bonded aggregates. Given the hydrophobic nature of the matrix, hydrogen bonds with the complex may only be established by the F atoms as electron donors, which is consistent with the shift observed in the νSi−F mode of the matrix from 760 to 754 cm^{-1}. Nevertheless, a new small band appears at 3562 cm^{-1} that, even for isolated 1,2,4-triazole molecules, is at a too high wavenumber
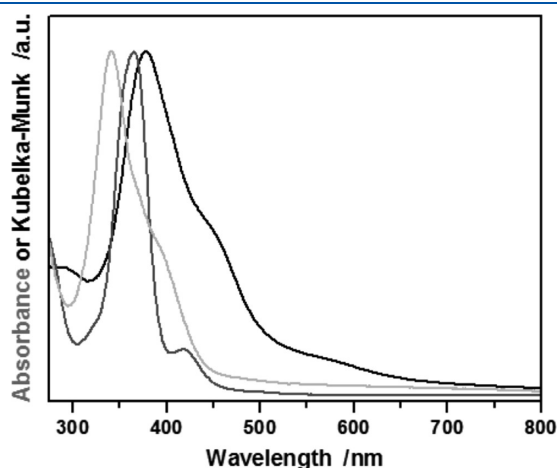
to account for non hydrogen bonded NH groups. This reveals the existence of some weakly H bonded hydroxyl groups, consistent with the partial ligand replacement by aquo/hydroxo groups.

Further insight on the processes undergone by the complex was obtained comparing the DRUV spectrum of the complex within the silica matrix to the UV spectra of fresh and aged acidic aqueous solutions (Figure 5).

The band profile of encapsulated *trans*-Htrz is similar to that of an acidic aqueous solution aged about 4 days, but broader and red-shifted. In the $300-600$ nm range, the spectrum of the fresh solution presents a strong band at 365 nm and a shoulder at 419 nm, both assigned to ligand-to-metal charge transfer (LMCT) transitions (Cl pπ → Ru dπ), typical of the *trans* Ru(III)−Cl$_4$ form of the complex.[20,34] After ~4 days, the spectrum shifts to the blue and the relative intensity of the shoulder increases, which may be interpreted in terms of an increase in the charge density of the metal center (eventually a reduction to Ru(II) induced by the medium or by linkage isomerization of one ligand), the two components being reassigned below.[5] The red shift observed within the silica matrix is ascribed to a confinement effect.

To estimate the level of modification induced on the complex, the spectra in Figure 5 were deconvoluted in a sum of Voigt components, using a nonlinear least-squares fitting method. The fitting details are available in Supporting Information (Figures S3−S5), and the results are included in Table 4 (first three rows).

In the aged acidic solution and in the encapsulated complex the LMCT bands decrease considerably in comparison with the fresh solution, and any remaining unaffected Ru(III) complex shows only one small LMCT component (5/7%) at 370 nm. For the encapsulated complex, the d−d transitions in Ru with higher charge density (Ru*) become the main components at 388 nm (70%) and 454 nm (16%), corresponding to those at 341 and 393 nm obtained for the aged acidic solution. This large shift is most certainly due to a matrix effect.[35] Moreover, some further reactions occurred while the matrix was forming, given the additional component retrieved at 566 nm (7%). This band confirms that aquation has occurred, yielding at least a mono-aquo/hydroxo Ru complex upon encapsulation. This result corroborates the presence of OH groups detected in the DRIFT spectra. A possible mechanism for the complex degradation during the sol−gel synthesis, where the first step is either the


Figure 5. Comparison of the DRUV spectrum of encapsulated *trans*-Htrz (black) with the UV−vis spectrum of *trans*-Htrz in acidic aqueous solution ([HCl] = 0.08 M): fresh (gray) and aged for 4 days (light gray).

Table 4. Results of the Band Deconvolution of the DRUV Spectra of Encapsulated and Co-Encapsulated (H$_2$trz)[*trans*-RuCl$_4$-(N^2-Htrz)$_2$] Complex and Purines: Wavelength (nm) and Relative Area (%) and Comparison with Aqueous Solutions

sample	purine[a]			Ru complex[b]			
	$\pi-\pi^*$	n−π^*	$\pi-\pi^*$	d−d (Ru*)[c]		LMCT (Cl → Ru^{III})	LMCT (H$_2$O/OH → Ru*)
trans-Htrz fresh aq soln						353 (56%) 370 (38%) 422 (6%)	
trans-Htrz acidic aq soln aged 4 days				341 (71%)	393 (24%)	370 (5%)	
trans-Htrz/SiO$_2$				388 (70%)	454 (16%)	370 (7%)	566 (7%)
Gua aq soln[22]	248 (70%)	272 (8%)	283 (12%)				
Gua/SiO$_2$	249 (39%)	292 (15%)	281 (46%)				
Gua/*trans*-Htrz/SiO$_2$	249 (50%)	276 (26%)	291 (24%)	389 (66%)	454 (19%)	369 (9%)	566 (7%)
Ade aq. soln[22]	251 (49%)		267 (51%)				
Ade/SiO$_2$	262 (83%)		277 (17%)				
Ade/*trans*-Htrz/SiO$_2$	260 (76%)		275 (24%)	394 (51%)	454 (20%)	368 (24%)	566 (5%)

[a] Relative areas (A_i) estimated as: $100 \times A_i/(\Sigma A_i)_{purine}$. [b] Relative areas ($A_j$) estimated as: $100 \times A_j/(\Sigma A_j)_{complex}$ [c] Ru* = Ru with higher charge density than Ru(III).
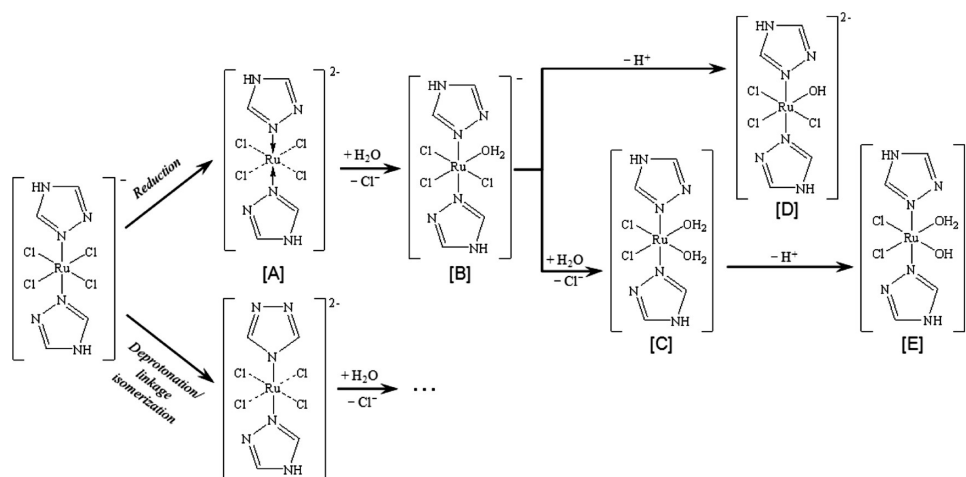
Figure 6. Schematic representation of proposed reaction paths undergone by encapsulated $(H_2trz)[trans\text{-}RuCl_4(N^2\text{-}Htrz)_2]$ during the sol−gel synthesis. Structure A stands for the species with increased charge density on the metal center, with nominal charge −2, and more labile Ru−Cl bonds.
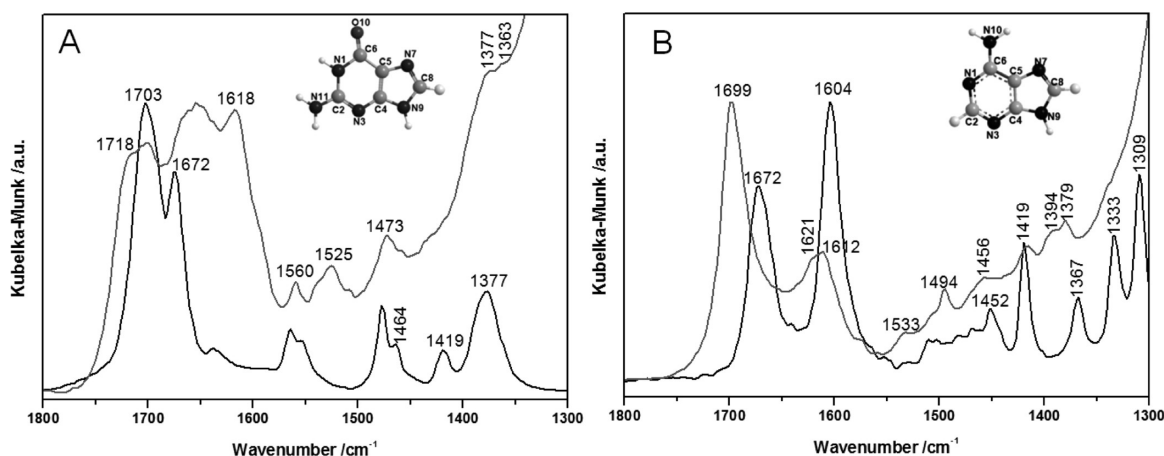
Figure 7. DRIFT spectra in the 1800−1300 cm^{-1} region of (A) crystalline Gua (black) and encapsulated within the silica matrix (gray), (B) crystalline Ade (black) and encapsulated within the silica matrix (gray). All the spectra were normalized to the maximum absorption.

reduction of Ru(III) to Ru(II) or the linkage isomerization of one ligand, is schematized in Figure 6.

As far as the DRIFT and DRUV spectra show, residual unreacted complex coexists within the matrix with species A, plus some aquated products that include species B−E or even further hydrolyzed forms.

The difference observed in the matrix pore morphology in comparison with the control silica may be justified by the interference of the various complex forms with the silica oligomers as the network builds.

3.3. Effects of Encapsulation on the DNA Purine Bases.
The infrared spectra of crystalline guanine and adenine and their UV spectra in aqueous solution have been analyzed in detail elsewhere.[21,22] The study of their interactions with coencapsulated trans-Htrz was preceded by a characterization of their behavior within this new fluorinated silica matrix.

The DRIFT spectrum of encapsulated Gua shows a very different profile from that of crystalline Gua (Figure.7A). The two components in the $\nu C{=}O$ band reveal that there are carbonyl groups interacting with other Gua molecules as in polycrystalline Gua (unshifted at 1703 cm^{-1}), as well as a significant population of less interacting ones (∼1718 cm^{-1}). The broad and composed $\delta(NH_2)$ band (∼1650−1580 cm^{-1}) indicates that there is a large fraction of almost free ammine groups (responsible for the component at 1618 cm^{-1}), while the others are involved in a variety of hydrogen bonds. Besides, only one kind of N9H exists, since the $\delta(N9H)$ doublet observed in crystalline Gua at 1564/1554 cm^{-1} appears as a single band at 1560 cm^{-1}. The absence of the band at 1419 cm^{-1}, assigned to $\nu(C4N9)$, and the new band at 1525 cm^{-1}, point to an increase in the CN bond order. These changes are consistent with a very low affinity of Gua to the matrix in terms of hydrogen bonding, but suggest a rather strong perturbation of the imidazole ring.[36] The splitting of the pyrimidinic $\delta(N1H)$ mode (at 1377 cm^{-1}) in a doublet at 1377/1363 cm^{-1} implies a fraction of freer N1H groups.

The broadening of the DRUV spectrum of encapsulated guanine and the inversion in the relative intensities of the two maxima in comparison with guanine in aqueous solution (Figure 8A) were interpreted taking into account the spectral deconvolution results (Table 4 and Figure S6 in Supporting Information). It becomes clear that the electron cloud of Gua is highly perturbed by encapsulation, as indicated by the following: (i) the intensities of the two $\pi{\rightarrow}\pi^*$ transitions (at 249 and 281 nm) change drastically, becoming very similar; (ii) the n−π^* transition shifts to the red

(from 272 to 292 nm), as a consequence of a lesser involvement of Gua electron lone pairs in hydrogen bonds, and their population increases comparatively to Gua in solution (15% instead of 8%).[37]

Both DRUV and DRIFT results show that encapsulated guanine is freer from hydrogen bonding interactions, as charge donor, than in solution and in crystalline phase: in fact, the carbonyl groups cannot establish hydrogen bonds with this hydrophobic fluorinated silica matrix; those can occur between fluorine and the ammine hydrogens of Gua, leaving most of the carbonyl oxygen atoms free or able to interact with other Gua molecules. Moreover, the repulsions between the carbonyl and fluorine lone electron pairs force entrapped Gua into orientations that render the highly directional NH···F hydrogen bonds less efficient and drastically change the possibility of $\pi-\pi$ interactions between Gua molecules. The lone pair−π interactions with the matrix fluorine atoms can also contribute to the perturbations observed in the resonant system of the purine.[38]

In contrast to the observed for Gua, the changes in the profile of the DRIFT spectrum of encapsulated adenine (Figure 7B)
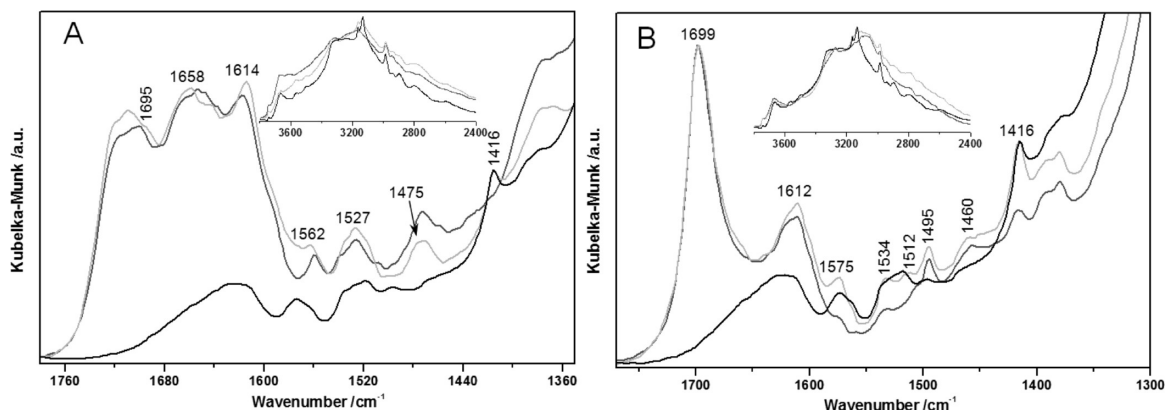
indicate stronger Ade-matrix hydrogen bonding than in polycrystalline Ade. The NH$_2$ deformation bands (at 1672 and 1604 cm^{-1} in polycrystalline Ade) shift to higher wavenumbers and the relative intensities of the two components invert. The shift is particularly large for the more interacting groups (27 cm^{-1}). A shoulder at ∼1621 cm^{-1} appears in the other component, differentiating the contributions of the $\delta(NH_2)$ and $\nu(C6C5)$ modes.[21] These changes imply that most ammine groups of adenine are involved in strong NH···F bonds with the matrix. The pattern related to the imidazole and pyrimidine rings modes (1550−1350 cm^{-1} region) is also much perturbed by encapsulation: the relative intensity of the $\nu(C4C5)$ (1419 cm^{-1}) mode decreases considerably, the pyrimidine ring stretching (1367 cm^{-1}) appears shifted as a doublet at 1394/1379 cm^{-1}, and new bands emerge at 1494 and 1533 cm^{-1} (assigned to $\delta(C8H)$ and $\nu(C4N9)$ modes shifted from 1508 cm^{-1} and with increased intensity). These ring perturbations are also apparent in the DRUV spectrum of encapsulated Ade (Figure 8B), which shifts to the red (5 nm) and broadens in comparison with that of Ade in solution. According to the spectral deconvolution results (Table 4 and Figure S7 in Supporting Information), this is due to the large shift of the $\pi-\pi^*$ transitions and to the drastic increase in the relative intensity of the lower energy component. This matrix effect on Ade is the opposite of what was observed on Gua, showing that π stacking between encapsulated Ade molecules is more efficient within the matrix. Such aggregation justifies the stronger effect of Ade on increasing the total pore volume of the matrix (Table 2), probably as a consequence of a modified pore morphology.
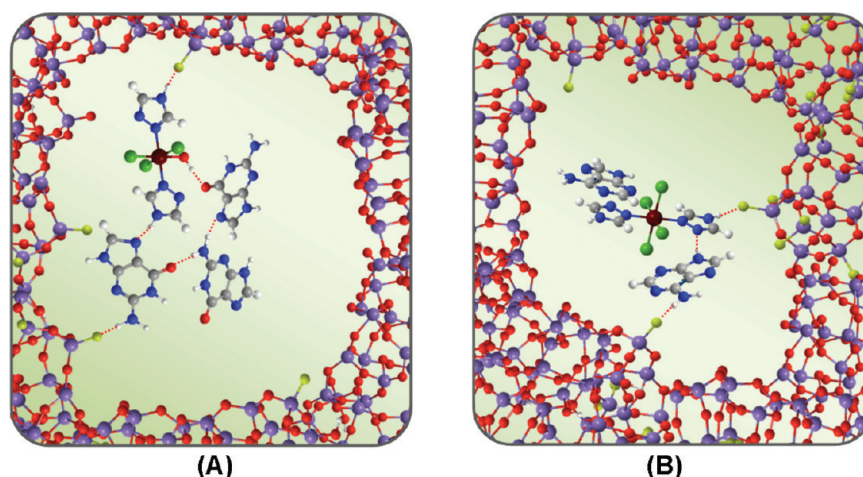
3.4. Interactions between Coencapsulated (H$_2$trz)[*trans*-RuCl$_4$(N^2-Htrz)$_2$] and the Purine Bases.
The superposition of the DRUV spectra of *trans*-Htrz encapsulated alone and coencapsulated with guanine (Figure 8C) shows that the presence of this purine does not interfere with the aquation processes undergone by the complex during the sol−gel reactions.

On the other hand, adenine induces some broadening and a red shift of the complex main band. By spectral deconvolution (Table 4 and Figure S8 in Supporting Information), this effect was understood in terms of a fraction of the Ru(III) complex being preserved: the relative intensity of the LMCT component at 368 nm increases from 7 to 24%, the sum of those related to the d−d transitions of the perturbed complex decrease, namely from

Figure 8. (A) UV spectrum of Gua in aqueous solution (black) and DRUV spectra of Gua/SiO$_2$ (gray) and Gua/*trans*-Htrz/SiO$_2$ (light gray); (B) UV spectrum of Ade in aqueous solution (black) and DRUV spectra of Ade/SiO$_2$ (gray) and Ade/*trans*-Htrz/SiO$_2$ (light gray); (C) DRUV spectra of *trans*-Htrz/SiO$_2$ (black), Ade/*trans*-Htrz/SiO$_2$ (gray) and Gua/*trans*-Htrz/SiO$_2$ (light gray).

Figure 9. DRIFT spectra of (A) encapsulated *trans*-Htrz (black), encapsulated Gua (gray) and coencapsulated Gua and complex (light gray), and (B) encapsulated *trans*-Htrz (black), encapsulated Ade (gray) and coencapsulated Ade and complex (light gray). Insets: detail of the spectra in the 3800−2400 cm^{-1} region, obtained with sample/KBr ratios 20 times higher. The spectra were normalized to the maximum absorption of purines (samples containing purines) and to the maximum absorption of the complex (samples containing complex).

Figure 10. Schematic representation of the proposed interactions between *trans*-Htrz and guanine (A) and *trans*-Htrz and adenine (B) coencapsulated within a fluorinated silica matrix: Ru (brown-red); Cl (green); Si (violet); O (red); N (blue); C (dark gray); H (light gray); F (olive).

86 to 71%, and the LMCT component due to aquo/hydroxo ligands from 7 to 5%. Either by direct interaction with the complex or by a modification of the medium,[39−41] Ade hinders the initial step of the complex degradation. Such preservation correlates with the different color observed for the Ade/complex solution in the first stages of the sol−gel process. The readjustment in the relative intensities of Ade $\pi-\pi^*$ bands when coencapsulated (Figure 8B and Table 4) may account for $\pi-\pi$ interactions with the complex triazole ligand.[42] These induce a decrease in the basicity of the ligand, and thus reduce the rate of the first chloride hydrolysis.[15,43]

The presence of the complex affects the DRUV spectrum of encapsulated Gua (Figure 8A) by increasing the relative intensity of the lower wavelength region. The components at 276 and 291 nm (Table 4 and Figure S9 in Supporting Information) were assigned to n−π^* and $\pi-\pi^*$ transitions, respectively, with the n−π^* transition shifted to the blue (16 nm) and with an enhanced intensity (26% versus 15%). This is consistent with stronger hydrogen bonding interactions of a larger fraction of electron lone pairs.[37] Besides, the π system of Gua is also perturbed by the coencapsulated complex, because the relative intensities of the $\pi-\pi^*$ transitions change toward those of Gua in aqueous solution and the lower energy transition shifts considerably to the red (∼10 nm with respect to encapsulated Gua).

The DRIFT spectra of samples Gua/*trans*-Htrz/SiO$_2$ and Ade/*trans*-Htrz/SiO$_2$ (Figure 9) allowed confirming this reasoning and band assignments. They are more informative on the modifications induced on the purines, given their higher content.

For coencapsulated Gua (Figure 9A), the νCO and δNH$_2$ bands become broader, with new components at ∼1695 and 1658 cm^{-1}, respectively, corroborating that there is a fraction of carbonyl and ammine groups more strongly hydrogen bonded than in Gua encapsulated alone. Since the matrix is essentially identical, these are established with the complex. Besides, the relative increase of the 1614 cm^{-1} component demonstrates that the fraction of ammine groups that have no access to the matrix also increases, due to the presence of the complex. The perturbation of the imidazole ring is visible from the broadening of the band at 1527 cm^{-1} (ν(CN)) and loss of the shoulder at 1464 cm^{-1} (δ(C8H)). The broadening of the 3800−2400 cm^{-1} region (inset in Figure 9A) to lower wavenumbers upon coencapsulation

may also be related to more strongly hydrogen bonded OH and NH groups. These directional Gua complex interactions contribute to the extremely high pore volume of the resulting silica structure that forms around the pair.

When Ade is coencapsulated with the complex (Figure 9B), the ammine groups establish the same types of strong hydrogen bonds with the matrix as when it is encapsulated alone, since the NH$_2$ scissors components at 1699 and 1612 cm^{-1} do not shift. However, the relative intensity of the δNH$_2$ at 1612 cm^{-1} increases. Thus, the fraction of the less interacting NH$_2$ groups increases due to the presence of the complex. Also the relatively strong band at 1575 cm^{-1} is assigned essentially to the δNH$_2$ mode of freer groups of Ade. In the region 1570−1350 cm^{-1}, some perturbations of the purine and triazole rings stand out: (i) the new maximum at 1512 cm^{-1} may be assigned to the ring stretching of the triazole ligands, shifted from 1518 cm^{-1}, and/or to a perturbed νC4N9 of Ade; (ii) the relative intensity of the δC8H (at 1495 cm^{-1}) increases; (iii) the splitting in the pyrimidine ring stretch doublet decreases (from 1394/1379 cm^{-1} to 1390/1381 cm^{-1}). Apparently, all the resonant system of adenine is more perturbed due to the presence of the complex, although no significant hydrogen bonding involving the NH$_2$ groups is established between the two molecules. These observations corroborate the existence of $\pi-\pi$ interactions between the rings of the two dopants, as suggested above. In the 3500−2400 cm^{-1} region (inset in Figure 9B), despite all the contributions from CH, NH, and OH stretching modes, there is a clear broadening to lower wavenumbers in comparison with the separately encapsulated components, which accounts for a larger proportion of more strongly hydrogen bonded NH groups (namely N4H/N9H of the complex and N9H of Ade), excluding the NH$_2$, as revealed by the analysis of their scissors mode.

Figure 10 summarizes the proposed complex−purine interactions.

4. CONCLUSIONS

The complementary information from UV−vis and infrared spectroscopies allowed studying the stability of the ruthenium complex triazolium [*trans*-tetrachlorobis(1*H*-triazole) ruthenate-(III)] in the restricted environment of a tailored sol−gel silica matrix, and its interactions with DNA purines (guanine and adenine).

1197

dx.doi.org/10.1021/jp210234e |*J. Phys. Chem. B* 2012, 116, 1189–1199

Controlled degradation of the complex was achieved by synthesizing a fluorinated, hydrophobic and extremely light silica matrix, prepared by a one-step sol—gel process at room temperature. However, it still undergoes a series of processes that lead to partial replacement of the chloride by aquo/hydroxo ligands, perturbing the ligand triazole rings. A possible decomposition pathway is proposed. The encapsulated complex interacts with the matrix by hydrogen bonds between the NH groups and the fluorine atoms (as charge donors), much weaker than those among complex molecules in the polycrystalline phase.

It was quantitatively demonstrated that coencapsulated Gua does not interfere with the processes undergone by the complex during the sol—gel reactions, but the two molecules interact by hydrogen bonding between the carbonyl and ammine groups of the purine and the NH and aquo groups of the complex. Also the imidazole rings of the purine are perturbed by the complex. In contrast, in the presence of Ade a fraction of the Ru(III) complex is preserved and the yield in the aquo complex is reduced. $\pi-\pi$ interactions between the triazole ligands of the complex and the pyrimidine and imidazole rings of Ade are established, as well as hydrogen bonds involving the N9H groups of the purine, but not most of its ammine groups.

Although the formation of adducts between methylated adenine and another Ru—azole complex was reported,[9] this type of covalent bonding has not been observed for triazole Ru complexes in aqueous solution, and the present study excludes that possibility within a confined environment of a silica matrix.

The real interactions of the Ru—triazole complex with DNA bases in living cells cannot be directly inferred from the present study, but these results strongly suggest that they involve hydrogen bonds of the types described above between the triazole, aquo, and/or hydroxo ligands and the imidazole ring (of both purines) and the pyrimidine ring (of adenine).

■ ASSOCIATED CONTENT

ⓢ Supporting Information. Figure S1, spectral deconvolution of the DRIFT spectrum of the control silica matrix in the $1000-1300$ cm^{-1} region; Figure S2, DRIFT spectrum of polycrystalline *trans*-Htrz; Figures S3 and S4, spectral deconvolution of the UV—vis spectra of aqueous solutions of *trans*-Htrz; Figures S5 to S9, spectral deconvolution of the DRUV spectra of encapsulated complex, adenine and guanine and of the coencapsulated molecules; and Table S1, results of the deconvolution in Figure S1. This material is available free of charge via the Internet at http://pubs.acs.org.

■ AUTHOR INFORMATION

Corresponding Author
*Telephone: +351-218419220. Fax: +351-218464455. E-mail: lilharco@ist.utl.pt.

■ ACKNOWLEDGMENT

■ REFERENCES

(1) Gasser, G.; Ott, I.; Metzler-Nolte, N. *J. Med. Chem.* **2011**, *54*, 3–25.

(2) Farrel, N. Metal Complexes as Drugs and Chemotherapeutic Agents. In *Comprehensive Coordination Chemistry II: From Biology to Nanotechnology*; McCleverty, J., Meyer, T., Eds.; Elsevier: Amsterdam, The Netherlands, 2005, Vol. 9, pp 809—840.

(3) Clarke, M. J. *Coord. Chem. Rev.* **2003**, *236*, 209–233.

(4) Frade, R. F. M.; Candeias, N. R.; Duarte, C. M. M.; André, V.; Duarte, M. T.; Gois, P. M. P.; Afonso, C. A. M. *Bioorg. Med. Chem. Lett.* **2010**, *20*, 3413–3415.

(5) Brindell, M.; Piotrowska, D.; Shoukry, A. A.; Stochel, G.; Eldik, R. *J. Biol. Inorg. Chem.* **2007**, *12*, 809–818.

(6) Bergamo, A.; Sava, G. *Dalton Trans.* **2007**, 1267–1272.

(7) Keppler, B. K.; Hartmann, M. *Metal-Based Drugs* **1994**, *1*, 145–149.

(8) Groessl, M.; Reisner, E.; Hartinger, C.; Eichinger, R.; Semenova, O.; Timerbaev, A. R.; Jakupec, M. A.; Arion, V. B.; Keppler, B. K. *J. Med. Chem.* **2007**, *50*, 2185–2193.

(9) Cebrián-Losantos, B.; Reisner, E.; Kowol, C. R.; Roller, A.; Shova, S.; Arion, V. B.; Keppler, B. K. *Inorg. Chem.* **2008**, *47*, 6513–6523.

(10) Hartinger, C. G.; Jakupec, M. A.; Zorbas-Seifried, S.; Groessl, M.; Egger, A.; Berger, W.; Zorbas, H.; Dyson, P. J.; Keppler, B. K. *Chem. Biodivers.* **2008**, *5*, 2140–2155.

(11) Bergamo, A.; Masi, A.; Jakupec, M. A.; Keppler, B. K.; Sava, G. *Metal-Based Drugs* **2009**, Article ID 681270, 9 pages.

(12) Hudej, R.; Turel, I.; Kanduser, M.; Scancar, J.; Kranjc, S.; Sersa, G.; Miklavcic, D.; Jakupec, M. A.; Keppler, B. K.; Cemazar, M. *Anticancer Res.* **2010**, *30*, 2055–2063.

(13) Reisner, E.; Arion, V. B.; Keppler, B. K.; Pombeiro, A. J. L. *Inorg. Chim. Acta* **2008**, *361*, 1569–1583.

(14) Chatlas, J.; Eldik, R.; Keppler, B. K. *Inorg. Chim. Acta* **1995**, *233*, 59–63.

(15) Küng, A.; Pieper, T.; Wissiack, R.; Rosenberg, E.; Keppler, B. K. *J. Biol. Inorg. Chem.* **2001**, *6*, 292–299.

(16) Resneir, E.; Arion, V. B.; Silva, M. F. C. G.; da; Lichtenecker, R.; Eichinger, A.; Keppler, B. K.; Kukushkin, V. Y.; Pombeiro, A. J. L. *Inorg. Chem.* **2004**, *43*, 7083–7093.

(17) Pieper, T.; Peti, W.; Keppler, B. K. *Metal-Based Drugs* **2000**, *7*, 225–232.

(18) Pieper, T.; Keppler, B. K. *Analusis Mag.* **1998**, *26*, 84–87.

(19) Huang, Y.-Q.; Ding, B.; Gao, H.-L.; Cheng, P.; Liao, D.-Z.; Yan, S.-P.; Jiang, A.-H. *J. Mol. Struct.* **2005**, *743*, 201–207.

(20) Arion, V. B.; Reisner, E.; Fremuth, M.; Jakupec, M. A.; Keppler, B. K.; Kukushkin, V. Y.; Pombeiro, A. J. L. *Inorg. Chem.* **2003**, *42*, 6024–6031.

(21) Lopes, L. M. F.; Garcia, A. R.; Fidalgo, A.; Ilharco, L. M. *Langmuir* **2009**, *25*, 10243–10250.

(22) Lopes, L. M. F.; Garcia, A. R.; Brogueira, P.; Ilharco, L. M. *J. Phys. Chem. B* **2010**, *114*, 3987–3998.

(23) Kubelka, P.; Munk, F. Z. *Tech. Phys.* **1931**, *12*, 593–601.

(24) Brinker, C. J.; Scherer, G. W. *Sol-Gel Science and Technology—The Physics and Chemistry of Sol-Gel Processing*; Academic Press: Boston, MA, 1990.

(25) Lataste, E.; Demourgues, A.; Leclerc, H.; Goupil, J.-M.; Vimont, A.; Durand, E.; Labrugère, C.; Benalla, H.; Tressaud, A. *J. Phys. Chem. C* **2008**, *112*, 10943–10951.

(26) Campostrini, R.; Ischia, M.; Carturan, G. *J. Sol.-Gel. Sci. Technol.* **2002**, *23*, 107–117.

(27) Zhu, W. X.; Gao, Y. X.; Zhang, L. Z.; Mao, J. C.; Zhang, B. R.; Duan, J. Q.; Qin, G. G. *Superlattice Microst.* **1992**, *12*, 409–412.

(28) Matos, M. C.; Ilharco, L. M.; Almeida, R. M. *J. Non-Cryst. Solids* **1992**, *147/148*, 232–237.

(29) Fidalgo, A.; Ilharco, L. M. *Chem.—Eur. J.* **2004**, *10*, 392–398.

(30) Mel'nikov, V. V.; Stolpakova, V. V.; Gidaspov, B. V. *Khim. Geterotsikl. Soedin.* **1972**, *11*, 1567–1570.

(31) Bougeard, D.; Le Calvé, N.; Saint Roch, B.; Novak, A. *J. Chem. Phys.* **1976**, *64*, 5152–5165.

(32) Malek, K.; Schroeder, G.; Proniewicz, L. M. *Vib. Spectrosc.* **2007**, *44*, 19–29.

(33) Claramunt, R. M.; López, C.; Garcia, M. A.; Otero, M. D.; Torres, M. R.; Pinilla, E.; Alarcón, S. H.; Alkorta, I.; Elguero, J. *New J. Chem.* **2001**, *25*, 1061–1068.

(34) Rack, J. J.; Gray, H. B. *Inorg. Chem.* **1999**, *38*, 2–3.

(35) Maruszewski, K.; Jasiorski, M.; Salamon, M.; Stręk, W. *Chem. Phys. Lett.* **1999**, *314*, 83–90.

(36) Muntean, C. M.; Puppels, G. J.; Greve, J.; Segers-Nolten, G. M. *J. Biopolymers (Biospectroscopy)* **2002**, *67*, 282–284.

(37) Fulscher, M. P.; Serrano-Andrés, L.; Roos, B. O. *J. Am. Chem. Soc.* **1997**, *119*, 6168–6176.

(38) Mooibroek, T. J.; Gamez, P.; Reedijk, J. *Cryst. Eng. Comm.* **2008**, *10*, 1501–1515.

(39) Joule, J. A.; Mills, K. *Heterocyclic Chemistry*, 5th ed.; Wiley: Chichester, U.K., 2010.

(40) Oliveira-Brett, A. M. L.; Silva, A.; Brett, C. M. A. *Langmuir* **2002**, *18*, 2326–2330.

(41) Cui, P. Y.; Meng, L. Q.; Liu, B. P. *Struct. Chem.* **2010**, *21*, 873–878.

(42) Hunter, C. A.; Singh, J.; Thornton, J. M. *J. Mol. Biol.* **1991**, *218*, 837–846.

(43) Iengo, E.; Mestroni, G.; Geremia, S.; Calligaris, S.; Alessio, E. *J. Chem. Soc., Dalton Trans.* **1999**, 3361–3371.